NJC

ROYAL SOCIETY OF CHEMISTRY

PAPER

View Article Online
View Journal

Check for updates

Cite this: DOI: 10.1039/c9nj06226b

Support morphology-dependent catalytic activity of the Co/CeO_2 catalyst for the aqueous-phase hydrogenation of phenol†

Jinzhi Lu,[ab] Zhanwei Ma,*[a] Xuemei Wei,[ab] Qinsheng Zhang[a] and Bin Hu*[a]

Received 16th December 2019,
Accepted 1st April 2020

DOI: 10.1039/c9nj06226b

rsc.li/njc

Herein, three Co/CeO_2 catalysts with various support morphologies were prepared by $Co_2(CO)_8$ decomposition at a low temperature of 180 °C on the ceria plane such as CeO_2 nanocubes (c-CeO_2), nanorods (r-CeO_2), and nanopolyhedrons (p-CeO_2). The Co/r-CeO_2 catalyst shows a much higher phenol conversion (82.5%) than Co/c-CeO_2 (47.9%) and Co/p-CeO_2 (24.7%) at 150 °C and 3 MPa H_2 in water. We demonstrate that the less hydrophilic Co/r-CeO_2 catalyst inhibits the adsorption of water and further promotes the adsorption of phenol. Moreover, the morphology effect and oxygen vacancies in different chemical environments of the support provide active sites for the dissociation and adsorption of phenol. The high concentration of oxygen vacancies exposed on the high active crystal plane leads to more efficient catalytic activity for the hydrogenation of phenol.

1. Introduction

The catalytic hydrogenation of phenol is a vital commercial petrochemical process for the synthesis of KA oil and is also recognized as a prototypical model reaction for upgrading the lignin-derived phenolic compounds to stable pyrolysis bio-oil.[1,2] In particular, cyclohexanol as an important product in the hydrogenation of phenol is widely used in the synthesis of nylon-6 and nylon 66, pharmaceuticals, plasticizers, surfactants, paints and industrial solvents.[3–5] As a result, much effort has been devoted to the developments of highly selective and efficient catalysts for phenol hydrogenation. For example, the supported Pd,[6] Pt,[7] Rh[8] and Ru[9] catalysts showed very high catalytic activity and selectivity for the hydrogenation of phenol. However, the venture for supply and volatile price of noble metals limited their practical applications. To address these problems, the development of catalysts based on the low-cost metals such as Fe, Co and Ni is promising for the phenol hydrogenation reaction. For example, the bimetallic Ni–Co encapsulated in a N-doped carbon matrix was employed to catalyse the hydrogenation of phenol, which exhibited >99.9% cyclohexanol conversion and selectivity in isopropanol.[10] Wang *et al.*[11] explored the hydrogenation of phenol on the CoO_x@CN catalysts, and this indicated that the synergistic effect between Co_3O_4 and the *in situ* generated Co^0 during the reaction greatly promoted the reaction. Although the Co_3O_4 played the role for the adsorption and activation of phenol and Co^0 was responsible for hydrogen adsorption and dissociation, the resulting metal–oxide interface is highly complicated, and it is difficult to determine the inherent interactions between the metal and the oxide support.

Recently, controlling the sample morphology with specific crystal planes has been proven to be a feasible strategy for the governable surface structure and electronic features. For example, ceria nanocrystals with uniform and well-defined planes, such as nanocubes ({100}), nanorods ({110} and {100}), and nanopolyhedra ({111} and {100}), have been controllably synthesized.[12–14] Ideally, the CeO_2(100) surface is terminated by an O layer. The CeO_2(110) and (111) surfaces have both exposed Ce^{4+} and O atoms.[15] Moreover, Nelson[16] found that the use of high-surface-area ceria as a support led to higher activity of phenol hydrogenation in comparison to the use of a low-surface-area one, and the mechanism of phenol adsorption and activation is related to the ceria surface geometry. Inspired by the use of nano-building blocks with the most amount of highly efficient planes, constructing the support for the catalyst with unique factors should be promising for enhancing the catalytic hydrogenation activity of phenol. However, to the best of our knowledge, the morphological effect of the support on the hydrogenation of phenol over supported Co catalysts has never been reported.

Herein, we effectively combine the ceria morphology effect and cobalt by the $Co_2(CO)_8$ decomposition at a low temperature of 180 °C on the ceria plane for constructing the Co/CeO_2

---

[a] *State Key Laboratory for Oxo Synthesis and Selective Oxidation, Lanzhou Institute of Chemical Physics, Chinese Academy of Sciences, Lanzhou 730000, China. E-mail: zhanweima@licp.cas.cn, hcom@licp.cas.cn; Fax: +86 931 8277088; Tel: +86 931 4968258*

[b] *University of Chinese Academy of Sciences, Beijing 100049, China*

† Electronic supplementary information (ESI) available. See DOI: 10.1039/c9nj06226b

catalysts. The facet effect led to the strong interaction between the Co metal and the support. Moreover, the less hydrophilic Co/r-CeO_2 catalyst can inhibit the adsorption of water and further promote the adsorption of phenol. And the high concentration of oxygen vacancies exposed on the high active crystal plane leads to more efficient catalytic activity for hydrogenation of phenol. The Co/r-CeO_2 catalyst shows much higher phenol conversion (82.5%) than Co/c-CeO_2 (47.9%) and Co/p-CeO_2 (24.7%) at 150 °C and 3 MPa H_2.

2. Experimental

2.1 Chemicals

All chemicals were purchased from Macklin Industrial Corporation in China. They were directly used without any further purification. All gases used in the experiment were 99.999% pure. The deionized water resistivity in all reactions was 18.25 MΩ cm.

2.2 Preparation of the support

The CeO_2 supports with different morphologies were prepared by a hydrothermal method.[17] Firstly, $Ce(NO_3)_3\cdot6H_2O$ (6.96 g) and NaOH (19.6 g) were dissolved in 5 mL and 35 mL of deionized water, respectively. Secondly, the two solutions were mixed without stirring and transferred directly to a 50 mL Teflon-lined stainless steel autoclave. Then, the mixture was heated at 100 °C and 180 °C for 24 hours to obtain r-CeO_2 and c-CeO_2, respectively. After hydrothermal treatment, the precipitate was washed with deionized water to pH = 7, then dried at 60 °C for 12 hours, and finally calcined at 450 °C for 4 hours in air at a heating rate of 2.5 °C min^{-1}. The p-CeO_2 nanoparticles were directly purchased.

2.3 Preparation of catalysts

All of the catalysts were prepared by a wetness impregnation method[18] and the cobalt loadings were 30 wt%. The preparation process is as follows: the CeO_2 supports with different morphologies (nanorods, nanocubes, and nanoparticles) were stirred in a solution of cobalt carbonyl $Co_2(CO)_8$ in hexane at room temperature for 12 h. Then a rotary evaporator was used to remove the solvent at 30 °C. The sample was calcined at 180 °C and in an N_2 atmosphere for 2 hours at a heating rate of 2.5 °C min^{-1}. Finally it was cooled to room temperature in an N_2 atmosphere.

2.4 Measurements of the catalytic activity

The hydrogenation reaction was carried out in a 50 mL stainless-steel high-pressure reactor. In general, phenol-(*p*-methyl phenol or guaiacol) (250 mg), catalyst (100 mg) and water (25 mL) are loaded into an autoclave. Then the reactor was purged with H_2 three times to remove air. Then the reactor was charged with 3 MPa H_2, and the reaction was run for 16 hours under stirring at 150 °C. After the reaction, the reactor was cooled to room temperature, and the remaining gas was carefully discharged. The reaction mixture was extracted with ethyl acetate and *n*-heptane as the internal standard. The content of the mixture was analyzed and the product was identified by GC-MS (Agilent Technologies 5975C and 7890A).

2.5 Characterization of the catalysts

X-ray powder diffraction (XRD) (X'pert PANalytical, Dutch) was used for the analysis of the crystalline structures of the samples, using Cu Kα radiation (λ = 1.54050 Å), 2θ ranges were 10°–90°. Transmission electron microscopy (TEM) images were obtained using a JEM-2010 with an acceleration voltage of 200 kV. X-ray photoelectron spectroscopy (XPS) analyses were performed on an X-ray photoelectron spectrometer (ESCALAB 250Xi) to detect the elemental compositions, and the electron binding energy scale of all spectra was calibrated using C 1s at 284.8 eV. UV-visible diffuse reflectance spectra were obtained using a UV-2550 (Shimadzu) spectrometer with $BaSO_4$ as the reference. The FT-IR spectra of the samples were recorded on a NEXUS 670 FT-IR spectrometer with KBr pellets prepared by manual grinding. Static water contact angles were measured using a DSA-100 optical contact angle meter (Kruss Company, Ltd, Germany). The temperature-programmed reduction (TPR) with H_2 was performed on a TP-5080 characterization instrument with a TCD detector. Prior to the TPR test, the 50 mg sample was pretreated at 300 °C for 1 hour in an Ar stream (27 mL min^{-1}) and then cooled to room temperature. The test was carried out by heating the sample (50 mg) from 25 °C to 900 °C in a H_2/Ar (H_2, 10%) mixture stream (30 mL min^{-1}) with a linear heating ramp of 10 °C min^{-1}. The temperature-programmed reduction (TPO) with O_2 was also performed on a TP-5080 characterization instrument with a TCD detector, and the test was carried out by heating the sample (50 mg) from 25 °C to 600 °C in a flow of O_2/Ar (O_2, 10%) mixture (30 mL min^{-1}) with a linear heating ramp of 10 °C min^{-1}.

3. Results & discussion

The Co/CeO_2 catalysts were fabricated by a two-step growth process. Briefly, CeO_2 supports with different morphologies were achieved by the hydrothermal method by tuning the NaOH concentration. Then, CeO_2 supports with different morphologies were immersed in the $Co_2(CO)_8$ hexane solution for adsorbing and forming the $Co(CO)_x$ species, and decomposed at 180 °C under a N_2 atmosphere. Fig. 1 and Fig. S1 (ESI†) show the transmission electron microscopy (TEM) images of the pure CeO_2 and Co/CeO_2 catalysts. The r-CeO_2 with a diameter of 8 ± 2 nm and a length of 100–300 nm (Fig. 1a) can be evidently observed in the figure, and the high resolution image (Fig. 1b) shows a clear (200) lattice fringe with an interplanar spacing of 0.27 nm, which is parallel to the nanorod stretching direction, indicating that r-CeO_2 is mainly enclosed by the (200) planes and preferentially grows along the (110) crystal orientation. c-CeO_2 is displayed in Fig. 1d with average sizes of approximately 50–300 nm and lattice spacings of 0.27 nm corresponding to the (100) facet (Fig. 1e). Fig. 1g shows that p-CeO_2 has an irregular shape that mainly exposes the (111) planes. From Fig. 1c, 1f and 1i,

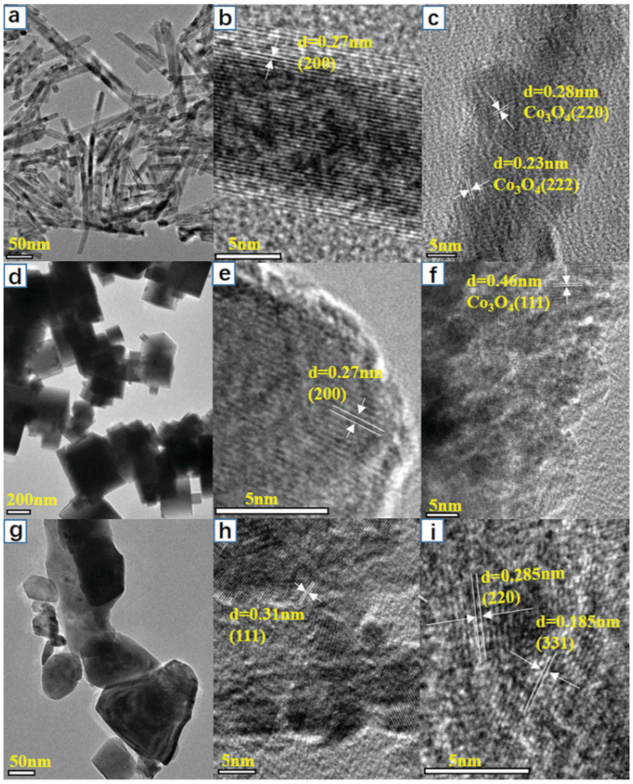

Fig. 1 TEM images of CeO_2 supports and their corresponding catalysts, (a and b) nanorods (r-CeO_2), (d and e) nanocubes (c-CeO_2), (g and h) nanoparticles (p-CeO_2), (c and f) Co/r-CeO_2 and Co/c-CeO_2, and (i) Co/p-CeO_2.

it can be noted that Co_3O_4 is formed on the r-CeO_2, c-CeO_2 and p-CeO_2 supports, respectively. The results indicated that the decomposition of $Co_2(CO)_8$ at 180 °C under a N_2 atmosphere led to the reaction with the surface oxygen or lattice oxygen in CeO_2. Moreover, the XRD patterns of the cobalt catalysts on CeO_2 supports with different morphologies are shown in Fig. S2 (ESI†). The main feature peaks can be ascribed to the diffraction patterns of the fluorite structure of CeO_2 (JCPDS: 34-0394). However, the diffraction peak of r-CeO_2 was wider than those of p-CeO_2 and c-CeO_2, which indicates the crystallinity is poor. The weak peaks at around 36.7° were assigned to Co_3O_4 (JCPDS: 01-1152), which is in accordance with the TEM results and the previous work.[19] From the TEM images and XRD patterns, we can see that no Co^0 is present on the catalysts. Considering that Co_3O_4 was the main metal phase in the catalysts, which cannot activate hydrogen, we should uncover the real active sites in the hydrogenation of phenol. To this end, we collected the reacted catalysts and used XRD and XPS to analyze the cobalt components in the different catalysts after the reaction. As shown in Fig. S3 (ESI†), except for the known crystal planes of CeO_2, the characteristic peak appearing at $2\theta = 44.3°$ is attributed to the Co^0 species (JCPDS: 01-1254). This indicates that cobalt oxide is reduced to Co^0 species during the reaction, which is consistent with the XPS of Co 2p (Fig. S4, ESI†) and the previous work.[11] For further verification, the used catalysts were dispersed in deionized water, and the solution became cloudy (Fig. S3a, ESI†). When a magnet is placed next to it, the catalyst is sucked to one side, and the solution becomes clear (Fig. S3b, ESI†), which suggested that the catalysts after the reaction exhibit magnetic properties indicating *in situ* generation of Co^0 under the reaction conditions at 150 °C and 3 MPa H_2. Moreover, the Co/r-CeO_2 catalyst after H_2 reduction showed a similar catalytic activity (Table S1, ESI†). Therefore, the *in situ* formation of Co^0 could provide the real active sites in the hydrogenation of phenol for activating hydrogen.

To illustrate the catalytic performance of the Co/CeO_2 catalysts, we select the hydrogenation of the phenol as a model reaction and also investigate the hydrogenation of other phenol derivatives. The hydrogenation of phenol reaction was carried out under the reaction conditions of 150 °C and 3 MPa H_2 using water as a solvent. From Fig. 2, it is clearly observed that the catalytic activity of Co/r-CeO_2 (82.5%) is much higher than those of Co/c-CeO_2 (47.9%) and Co/p-CeO_2 (24.7%) catalysts in the phenol hydrogenation reaction. When the reaction temperature was 130 °C, different cobalt-based catalysts also showed the same tendency. However, the synthesized CeO_2 (r-CeO_2, c-CeO_2 and p-CeO_2) supports showed no activity and the activity of phenol hydrogenation catalyzed by Co_3O_4 is not high (26.5%) (Table S1, ESI†), indicating that the CeO_2 support has a great influence on the phenol hydrogenation reaction. Table S1 (ESI†) also shows the results of the hydrogenation of phenol derivatives using Co/r-CeO_2 catalysts. As it can be seen, the catalytic activity of Co/r-CeO_2 for the hydrogenation of guaiacol (40%) and *p*-cresol (56%) was lower than that for phenol (82.5%). When the substitution of the aromatic ring was varied, the conversions of the reactions were different, which was because the presence of methyl and methoxy groups makes it difficult to decrease the electron density on the aromatic ring.

In order to study the reasons for the difference in the catalytic activity, a series of characterization studies were performed. As the specific crystal planes have different surface electronic and structural features, the surface chemical states of Ce, O and Co elements in three Co/CeO_2 catalysts were investigated. Fig. 3 shows the high-resolution O 1s XPS spectra.

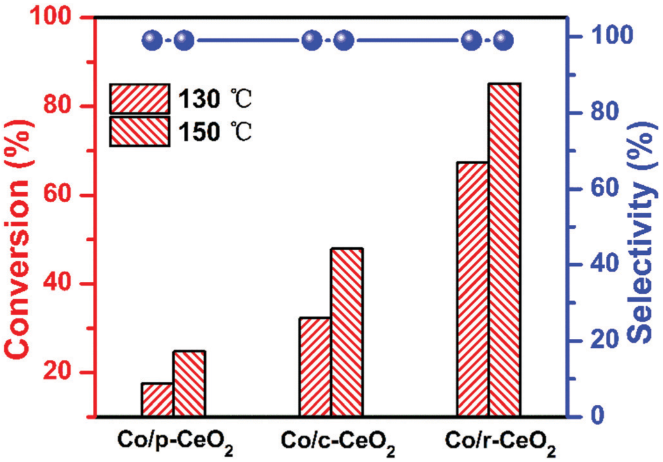

Fig. 2 Catalytic hydrogenation of phenol using different Co-based catalysts at different temperatures.

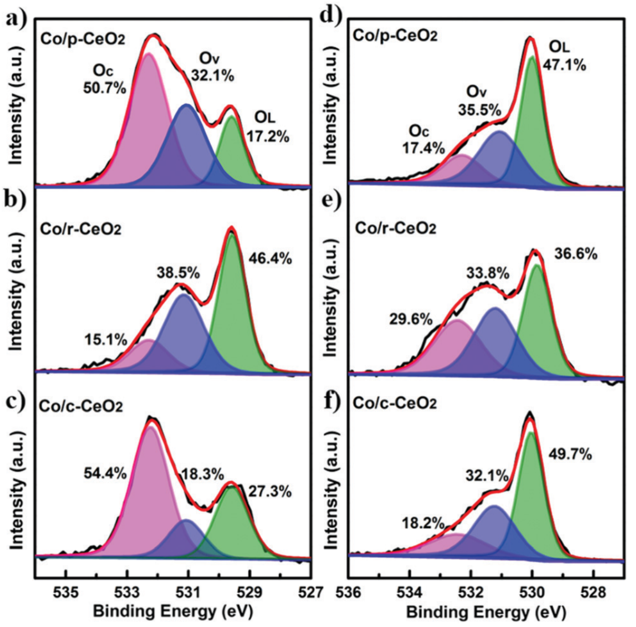

Fig. 3 O 1s XPS spectra of Co/p-CeO_2, Co/r-CeO_2 and Co/c-CeO_2 catalysts before (a–c) and after the reaction (d–f).

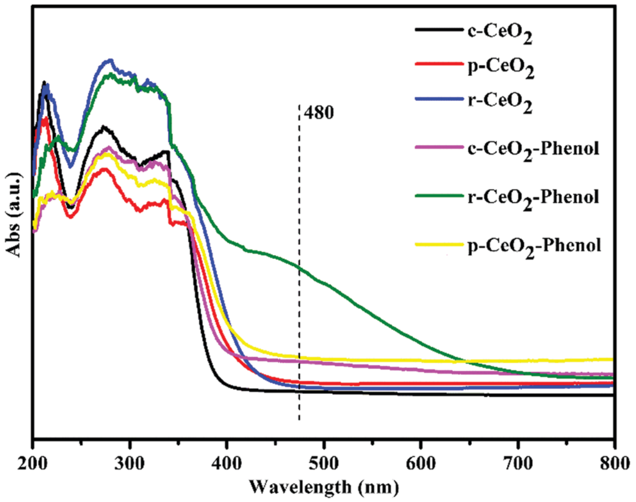

Fig. 4 UV-vis diffuse reflectance spectra of the CeO_2 supports with different morphologies and CeO_2 adsorbed with phenol.

The O 1s XPS spectra exhibit three peaks at 529.4 eV (O_L), 531 eV (O_V), and 532.4 eV (O_C), which are assigned to the lattice oxygen bound to the metal cations, O^{2-} in the oxygen-deficient regions, and chemisorbed or dissociated oxygen species or OH, respectively.[20] Interestingly, the amount of O_C was much larger in Co/p-CeO_2 and Co/c-CeO_2 than that in Co/r-CeO_2, which suggested that the chemisorbed or dissociated oxygen species or OH were more easily adsorbed on p-CeO_2 and c-CeO_2 than r-CeO_2. Moreover, in the FT-IR spectra (Fig. S5, ESI†), the peak at 1628 cm^{-1} was indexed to H_2O, and these results indicated that the Co/p-CeO_2 and Co/c-CeO_2 catalysts can adsorb water, which was coincident with the results of static water contact angles measurement for Co-based catalysts (Fig. S6, ESI†), where the contact angle of Co/r-CeO_2 (43.7°) catalysts is larger than those of Co/c-CeO_2 (20.4°) and Co/p-CeO_2 (20.1°) catalysts. The above results illustrate that the Co/c-CeO_2 and Co/p-CeO_2 catalysts were more hydrophilic than the Co/r-CeO_2 catalyst. Additionally, Ma *et al.*[17] reported that the zeta potentials of r-CeO_2, c-CeO_2, and p-CeO_2 are different and relate to the surface atom arrangement. Therefore, the competitive adsorption of phenol and water on Co/CeO_2 catalysts could affect the activity of phenol hydrogenation.

Moreover, the UV-vis diffuse reflectance measurements were used to investigate the adsorption of phenol on CeO_2 in water. In Fig. 4, it can be clearly seen that there is a higher absorbance (λ_{max} = 480 nm) in r-CeO_2–phenol, which is an indication of higher amounts of phenoxy species. However, the absorbance peak of phenoxy species was much weaker in c-CeO_2–phenol and p-CeO_2–phenol, which indicated that the hydrophilic Co/c-CeO_2 and Co/p-CeO_2 catalysts prefer to adsorb water, which led to a decrease in the adsorption of phenol on these catalysts. As Co/r-CeO_2 was less hydrophilic, it can inhibit the adsorption of water and further promote the adsorption of phenol on the catalyst. Moreover, these results were also supported by the reports on the construction of the hydrophilic or hydrophobic CeO_2 with different morphologies.[21,22]

To deeply gain insight into the competitive adsorption of phenol and water on Co/CeO_2, the effect of solvent on the reaction was investigated (Table S2, ESI†). It can be obviously noted that the solvent enormously affected the performance of the Co/r-CeO_2 catalyst. In *n*-hexane, the conversion of phenol was 86.2%, which was the highest among the solvents. Ethanol and i-propanol showed higher activity than water. These results further indicated that the less hydrophilic properties of the Co/r-CeO_2 catalyst promoted competitive adsorption of phenol on the facet of CeO_2 in water. Ethanol and i-propanol can also adsorb on the catalyst, while the –OH group was much more weakly bound to the CeO_2 surface than the OH^- of water. Additionally, the conversions of phenol in THF and dimethyl sulfoxide were 21.8% and trace, respectively, so it can be concluded that the activity of the catalyst was also related to the solvent polarity. Then, catalyst recycling experiments were performed in hexane (Fig. S7, ESI†). The conversion decreased to 10% after the sixth cycle. Interestingly, the catalytic activity could be fully restored after regeneration. Additionally, the FTIR spectra of the used Co/r-CeO_2 catalyst showed strong peaks at 3508–3024 cm^{-1} assigned to adsorbed phenyl species and at 2865, 2806, 1403 and 1157 cm^{-1} assigned to the cyclohexyl species (Fig. S8, ESI†). Consequently, the decreased activity in *n*-hexane may be ascribed to the adsorption of phenol and desorption of cyclohexanol, and the weaker polarity of *n*-hexane is unfavourable for the desorption of cyclohexanol. In water, the catalytic activity of the regenerated catalyst was close to that of the fresh catalyst and the morphologies were well maintained (Fig. S9, ESI†). The conversion mildly decreased by about 6% after 8 runs due to the loss of the catalyst during the recovery. Therefore, the solvent could affect the adsorption of phenol and desorption of cyclohexanol on the coordinatively unsaturated cerium cations or oxygen vacancies.

The number of surface oxygen vacancies can be roughly estimated based on the ratio of O_V/O_L.[23] As shown in Table S3 (ESI†), after the reaction, the ratio of O_V/O_L on the Co/r-CeO_2 (0.9) catalyst is higher than that of Co/c-CeO_2 (0.7) and Co/p-CeO_2 (0.65), which means that the Co/r-CeO_2 catalyst has more oxygen vacancies than Co/c-CeO_2 and Co/p-CeO_2. As the Ce^{3+} is closely related to the oxygen vacancy, the Ce species should be discussed. There are two types of cerium oxides present, as shown in Fig. S10 (ESI†), Ce^{3+} and Ce^{4+}. The amount of Ce^{3+} is estimated to be 34%, 26.2% and 27.2% for Co/r-CeO_2, Co/c-CeO_2 and Co/p-CeO_2 (Table S3, ESI†), respectively. The high concentration of Ce^{3+} ions on the surface of the Co/r-CeO_2 sample reflects the high concentration of surface oxygen vacancies. Numerous studies[24] have shown that the dissociative adsorption of phenol mainly occurs on the support, while the metal mainly activates the hydrogen. Moreover, Nelson *et al.*[16] reported that the adsorption and activation of phenol occurs on the ceria support and the mechanism is related to the ceria surface geometry. They suggested that coordinately unsaturated cerium cations near hydroxyl groups may be the active sites for the reaction. Therefore, the concentration of oxygen vacancies depending on the morphology of CeO_2 is vital to the catalytic hydrogenation of phenol. Considering that the concentration of surface oxygen vacancies on Co/c-CeO_2 and Co/p-CeO_2 are similar, the differences in their catalytic performance should be attributed to the different facets on which they are exposed. The ideal CeO_2(100) surface is a polar plane and its surface is terminated by an O layer. The CeO_2(110) and (111) surfaces are nonpolar planes (charge neutral) and their surfaces have both exposed Ce^{4+} and O atoms (Fig. S11, ESI†). The oxygen vacancies on different crystal planes are in different chemical environments, resulting in different activities. Although the oxygen vacancies on Co/p-CeO_2 are more than those on Co/c-CeO_2, p-CeO_2 mainly exposes the (111) crystal plane, and its activity is worse than that of the (100) crystal plane, resulting in weaker activity of the oxygen vacancies on p-CeO_2 than that on c-CeO_2. Therefore, the phenol hydrogenation activity is related to the oxygen vacancies located in the chemical environment.

Furthermore, H_2-TPR was used to explore the reduction behaviour of the catalysts. In general, the reduction peak of CeO_2 can be divided into three temperature zones: 250–400 °C, 400–600 °C and 600–900 °C, which represent the reduction of surface oxygen species, subsurface oxygen species and bulk lattice oxygen.[25,26] Fig. 5 shows the H_2-TPR profiles of the CeO_2 supports with different morphologies and the supported Co catalysts. The peaks in high temperature regions ($>$600 °C) can be attributed to the reduction of lattice oxygen of bulk CeO_2. The r-CeO_2, c-CeO_2 and p-CeO_2 supports exhibit the reduction peaks at 113 °C, 487 °C and 383 °C, respectively, which could be attributed to the reduction of CeO_2 surface oxygen. Interestingly, the surface oxygen reduction temperature of the support clearly varied, which indicated the oxygen in the (100) plane formed stronger chemical bonds with Ce than that in (110) and (111) planes. These results imply that the oxygen located on the facets have different oxygen vacancy formation energies. After Co species loading, the reduction peak of the supports shifted to the low temperature region, due to the strong interaction between the metal and the CeO_2 support, which greatly weakens the Ce–O bond at the contact with the metal and enhances its oxygen reduction performance.

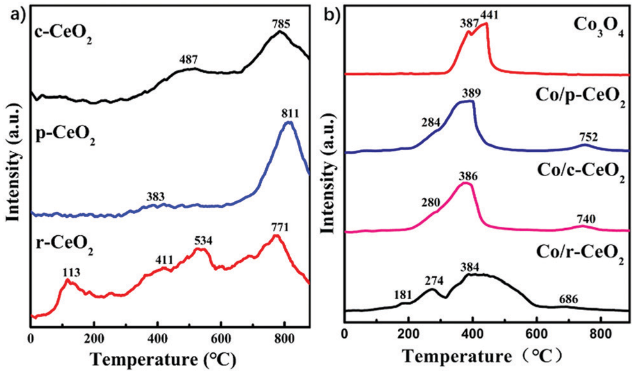

Fig. 5 H_2-TPR profiles of the CeO_2 supports with different morphologies (a) and the supported Co catalysts (b).

In addition, the programmed temperature oxidation (TPO) of Co/CeO_2 catalysts with three different morphological supports were also investigated (Fig. S12, ESI†). When the three catalysts are heated from 0 °C to 600 °C, oxygen consumption peaks appear between 380 °C and 400 °C. The Co/c-CeO_2 also shows an oxygen consumption peak at around 61 °C, which could be attributed to the oxidation of CoO_X. The intensity of the oxygen consumption peak is related to the oxygen vacancy and the Ce^{3+} concentrations. It can be seen that Co/r-CeO_2 has the strongest oxygen consumption peak, followed by Co/c-CeO_2 and Co/p-CeO_2, indicating that the oxygen vacancy and the Ce^{3+} concentrations are ranked in the order: Co/r-CeO_2 $>$ Co/c-CeO_2 $>$ Co/p-CeO_2, which is in accordance with the XPS results.

On the basis of the above results, the structure–activity relationship between the Co/CeO_2 catalysts and the hydrogenation of phenol reaction in water could be ascribed to the following reasons: firstly, the different facets of CeO_2 have varied surface structures and electronic features such as the number of oxygen vacancies and chemical environments. Moreover, the Co/c-CeO_2 and Co/p-CeO_2 catalysts were more hydrophilic than the Co/r-CeO_2 catalyst. The competitive adsorption of phenol and water on the surface active sites of CeO_2 affects the dissociation and adsorption of phenol. The metal Co nanoparticles were responsible for hydrogen adsorption and dissociation and further reaction for the adsorption and activation of phenol on the facet of CeO_2.

Conclusions

In summary, we immersed CeO_2 supports with different morphologies into $Co_2(CO)_8$ hexane solution and decomposed it at 180 °C to form the Co/CeO_2 catalysts. The obtained catalysts were successfully applied for the hydrogenation of phenol into cyclohexanol. The Co/r-CeO_2 catalyst shows much higher phenol conversion (82.5%) than Co/c-CeO_2 (47.9%) and Co/p-CeO_2

(24.7%) at 150 °C and 3 MPa H_2. The synergistic effect between the Co nanoparticles and the CeO_2 morphology during the reaction greatly promoted the reaction. Moreover, compared with the (111) and (100) plane, exposing the (110) facets on the r-CeO_2 with more active oxygen vacancies and the less hydrophilic properties enhances the dissociation and adsorption of phenol. And this work confirms the importance of support morphology on the hydrogenation of phenol using non-noble metal based catalysts.

Conflicts of interest

There are no conflicts to declare.

Acknowledgements

This research was financially supported by the CAS ''Light of West China'' Program.

Notes and references

1 N. Yan, Y. Yuan, R. Dykeman, Y. Kou and P. J. Dyson, *Angew. Chem., Int. Ed.*, 2010, **49**(32), 5549–5553.

2 K. L. Luska, P. Migowski, S. El Sayed and W. Leitner, *Angew. Chem., Int. Ed.*, 2015, **54**(52), 15750–15755.

3 S. Van de Vyver and Y. Roman-Leshkov, *Catal. Sci. Technol.*, 2013, **3**(6), 1465–1479.

4 H. Zhang, A. Han, K. Okumura, L. Zhong, S. Li, S. Jaenicke and G. K. Chuah, *J. Catal.*, 2018, **364**, 354–365.

5 P. Makowski, R. D. Cakan, M. Antonietti, F. Goettmann and M. M. Titirici, *Chem. Commun.*, 2008, 999–1001.

6 G. Yang, J. Zhang, H. Jiang, Y. Liu and R. Chen, *Appl. Catal., A*, 2019, **588**, 117306.

7 N. Singh, M. S. Lee, S. A. Akhade, G. Cheng, D. M. Camaioni, O. Y. Gutierrez, V. A. Glezakou, R. Rousseau, J. A. Lercher and C. T. Campbell, *ACS Catal.*, 2019, **9**(2), 1120–1128.

8 S. I. Fujita, T. Yamada, Y. Akiyama, H. Cheng, F. Zhao and M. Arai, *J. Supercrit. Fluids*, 2010, **54**(2), 190–201.

9 V. Vinokurov, A. Glotov, Y. Chudakov, A. Stavitskaya, E. Ivanov, P. Gushchin, A. Zolotukhina, A. Maximov, E. Karakhanov and Y. Lvov, *Ind. Eng. Chem. Res.*, 2017, **56**(47), 14043–14052.

10 A. Li, K. Shen, J. Chen, Z. Li and Y. Li, *Chem. Eng. Sci.*, 2017, **166**, 66–76.

11 Z. Wei, Y. Li, J. Wang, H. Li and Y. Wang, *Chin. Chem. Lett.*, 2018, **29**(6), 815–818.

12 K. Kaneko, K. Inoke, B. Freitag, A. B. Hungria, P. A. Midgley, T. W. Hansen, J. Zhang, S. Ohara and T. Adschiri, *Nano Lett.*, 2007, **7**(2), 421–425.

13 C. Pan, D. Zhang, L. Shi and J. Fang, *Eur. J. Inorg. Chem.*, 2008, (15), 2429–2436.

14 Y. Liu, Z. Li, H. Xu and Y. Han, *Catal. Commun.*, 2016, **76**, 1–6.

15 H. F. Wardenga and A. Klein, *Appl. Surf. Sci.*, 2016, **377**, 1–8.

16 N. C. Nelson, J. S. Manzano, A. D. Sadow, S. H. Overbury and I. I. Sowing, *ACS Catal.*, 2015, **5**(4), 2051–2061.

17 Z. Ma, S. Zhao, X. Pei, X. Xiong and B. Hu, *Catal. Sci. Technol.*, 2017, **7**(1), 191–199.

18 L. Zhu, S. Shan, V. Petkov, W. Hu, A. Kroner, J. Zheng, C. Yu, N. Zhang, Y. Li, R. Luque, C.-J. Zhong, H. Ye, Z. Yang and B. H. Chen, *J. Mater. Chem. A*, 2017, **5**, 7869–7875.

19 L. Zhu, Z. Yang, J. Zheng, W. Hu, N. Zhang, Y. Li, C.-J. Zhong, H. Ye and B. H. Chen, *J. Mater. Chem. A*, 2015, **3**, 11716–11719.

20 D. Liu, G. Li, F. Yang, H. Wang, J. Han, X. Zhu and Q. Ge, *J. Phys. Chem. C*, 2017, **121**(22), 12249–12260.

21 G. M. Lyu, Y. J. Wang, X. Huang, H. Y. Zhang, L. D. Sun, Y. J. Liu and C. H. Yan, *Nanoscale*, 2016, **8**(15), 7923–7932.

22 L. Hu, X. Song, X. Shan, X. Zhao, F. Guo and P. Xiao, *ACS Appl. Mater. Interfaces*, 2019, **11**(40), 37209–37215.

23 Z. Hu, X. Liu, D. Meng, Y. Guo, Y. Guo and G. Lu, *ACS Catal.*, 2016, **6**, 2265–2279.

24 X. Kong, Y. Gong, S. Mao and Y. Wang, *ChemNanoMat*, 2018, **4**(5), 432–450.

25 J. Manuel Lopez, A. L. Gilbank, T. Garcia, B. Solsona, S. Agouram and L. Torrente-Murciano, *Appl. Catal., B*, 2015, **174**, 403–412.

26 W. Mista, M. A. Malecka and L. Kepinski, *Appl. Catal., A*, 2009, **368**(1-2), 71–78.